Showcasing research from the International Tomography Center SB RAS (Russia), the Novosibirsk State University (Russia), the University of Helsinki (Finland), the Hungarian Academy of Sciences (Hungary) and the University of Oulu (Finland)

Title: Nuclear spin hyperpolarization with *ansa*-aminoboranes: a metal-free perspective for parahydrogen-induced polarization

This paper reports a series of unimolecular metal-free frustrated Lewis pairs based on an *ansa*-aminoborane (AAB) moiety, allowing observation of nuclear spin hyperpolarization effects upon interaction with parahydrogen. Hyperpolarization was observed for all AABs differing in boryl site substituent (−H, −Ph, −*o*-iPr-Ph, −Mes) in a wide temperature range. A theoretical analysis revealed the roles of chemical exchange, chemical equilibrium and spin dynamics in terms of the key parameters, providing a foundation for design of metal-free tweezer-like molecules for parahydrogen-induced polarization.

PAPER

Nuclear spin hyperpolarization with *ansa*-aminoboranes: a metal-free perspective for parahydrogen-induced polarization†

Vladimir V. Zhivonitko,*[ab] Kristina Sorochkina,[c] Konstantin Chernichenko,[c] Bianka Kótai,[d] Tamás Földes,[d] Imre Pápai,[d] Ville-Veikko Telkki,[e] Timo Repo[c] and Igor Koptyug[ab]

The parahydrogen-induced polarization (PHIP) phenomenon, observed when parahydrogen is used in H_2 addition processes, provides a means for substantial NMR signal enhancements and mechanistic studies of chemical reactions. Commonly, noble metal complexes are used for parahydrogen activation, whereas metal-free activation is rare. Herein, we report a series of unimolecular metal-free frustrated Lewis pairs based on an *ansa*-aminoborane (AAB) moiety in the context of PHIP. These molecules, which have a "molecular tweezers" structure, differ in their substituents at the boryl site (–H, –Ph, –*o*-iPr-Ph, and –Mes). PHIP effects were observed for all the AABs after exposing their solutions to parahydrogen in a wide temperature range, and experimental measurements of their kinetic and thermodynamic parameters were performed. A theoretical analysis of their nuclear spin polarization effects is presented, and the roles of chemical exchange, chemical equilibrium and spin dynamics are discussed in terms of the key dimensionless parameters. The analysis allowed us to formulate the prerequisites for achieving strong polarization effects with AAB molecules, which can be applied for further design of efficient metal-free tweezers-like molecules for PHIP. Mechanistic (chemical and physical) aspects of the observed effects are discussed in detail. In addition, we performed quantum chemical calculations, which confirmed that the *J*-coupling between the parahydrogen-originated protons in AAB–H_2 molecules is mediated through dihydrogen bonding.

[a] *Laboratory of Magnetic Resonance Microimaging, International Tomography Center SB RAS, Institutskaya St. 3A, 630090 Novosibirsk, Russia. E-mail: v_zhivonitko@tomo.nsc.ru*
[b] *Department of Natural Sciences, Novosibirsk State University, Pirogova St. 2, 630090 Novosibirsk, Russia*
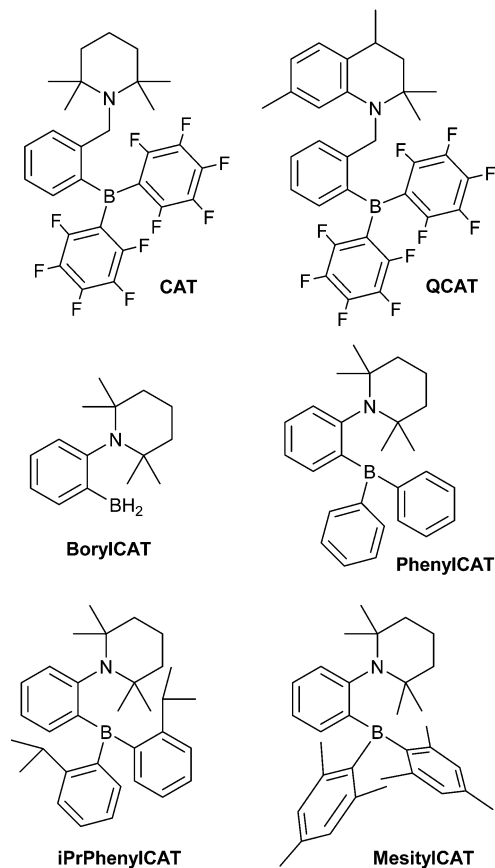[c] *Department of Chemistry, University of Helsinki, A. I. Virtasen Aukio 1, 00014 Helsinki, Finland*
[d] *Research Centre for Natural Sciences, Hungarian Academy of Sciences, Magyar Tudósok Körútja 2, H-1117 Budapest, Hungary*
[e] *NMR Research Unit, University of Oulu, P.O. Box 3000, 90014 Oulu, Finland*

† Electronic supplementary information (ESI) available: Full sets of ^{1}H NMR spectra measured with AABs at variable temperatures after para-H_2 bubbling; Eyring plots used for extraction of energetic parameters from k_{dis} at variable temperatures; evaluation of analytical expression for $I_z^{NH} \cdot I_z^{BH}$ spin order strength accumulated during para-H_2 bubbling by AAB–H_2 compounds; preparation procedures and characterization spectra; details of quantum chemical computations; table of calculated PHIP signal attenuation factors for the AABs under study. See DOI: 10.1039/c6cp05211h

1. Introduction

The high reactivity of frustrated Lewis pairs (FLPs) was discovered only recently,[1,2] inspiring numerous brilliant studies in this field over the last few years.[3–12] Many small molecules have been shown to be activated by FLPs,[6,12] including dihydrogen (H_2). In addition to the apparent applications in catalysis,[13–24] addition of H_2 to FLPs may be useful for hyperpolarizing nuclear spins when parahydrogen, one of the nuclear spin isomers of H_2, is used as a reagent. Due to the symmetry of the H_2 molecule, the correlation of its nuclear spins survives for a long time and can be transformed into observable nuclear spin hyperpolarization upon a chemical transformation of H_2 molecules if this transformation causes the two hydrogens to be magnetically inequivalent. At the same time, the H_2 activation mechanism must be pairwise, meaning that both hydrogens should follow each other throughout all elementary reaction steps and end up in the same product molecule. Because of this prerequisite, only certain catalytic systems are applicable in this hyperpolarization technique, which is referred to in the literature as PASADENA,[25] ALTADENA,[26] or, generally, parahydrogen-induced polarization (PHIP).[27] To date, PHIP mediated by FLPs was demonstrated only in a few examples as a proof-of-principle.[28,29] In particular, it has been shown that the reversibility of the H_2 interaction with FLPs allows one to achieve reproducible nuclear spin hyperpolarization each time the parahydrogen flux is introduced to a QCAT *ansa*-aminoborane

Scheme 1 *ansa*-Aminoboranes which have been shown to enable PHIP observation in previous work[28] (CAT and QCAT) and herein (BorylCAT, PhenylCAT, iPrPhenylCAT and MesitylCAT).

solution (Scheme 1), imitating a kind of nuclear spin polarization "pumping".[28]

In addition to the production of nuclear spin hyperpolarization for substantial signal enhancement in NMR and MRI, PHIP can shed light on the mechanistic features of molecular activation. Particularly, parahydrogen provides a unique type of labeling which is sensitive to the pairwise mechanism. At the same time, progress in understanding the involved mechanisms can provide a means for the development of new efficient FLP systems for PHIP. In particular, determination and optimization of the kinetic parameters of the activation are also crucial for maximizing PHIP. Unlike the spin correlation in parahydrogen, the lifetime of nuclear spin polarization in FLP–H_2 adducts is relatively short, which strongly diminishes the achievable polarization levels if the kinetics of the hydrogen addition is slow. This actually means that high addition rates compared to the spin relaxation rates are favorable for the observation of high polarization levels.

Recently, we reported that *ansa*-aminoboranes (AABs), N–B based FLPs, demonstrate PHIP effects, indicating that these compounds possess the required properties.[28] The chelating arrangement of the N and B reactive centers in AABs favors rapid H_2 addition dynamics. Importantly, the intrinsic feature of AABs is the presence of a dihydrogen NH···HB bond in the

AAB–H_2 adducts. This bond is evident from X-ray and neutron diffraction studies[30] and from computational results. Thus, AABs are referred to in the literature as "molecular tweezers" that stretch, but do not completely split, H_2 molecules. As shown below, the dihydrogen bond enables the observation of PHIP. Apparently, with further development, AABs may have great prospects in PHIP production. Namely, an appropriate molecular design could allow one to use close-to-ambient temperatures and, as an ultimate goal, to design moisture-tolerant AABs for *in vivo* MRI applications. Fundamentally, molecular activation with these compounds is of exceptional interest for metal-free catalysis as a new area with major potential for significant future advances.

Switching from the originally developed AABs, which were based on the 2-boryl-benzylamine core, to 2-aminophenyl-boranes provided more favorable thermodynamics of H_2 addition.[31] Due to its unique properties, which enable unprecedented catalytic hydrogenations[11] and C–H borylations,[32,33] the 2-aminophenylboryl core allowed us to design novel AABs with substituents other than C_6F_5 at the boryl site. Particularly, we have recently reported that BorylCAT, the AAB with the smallest boryl site (–BH_2), also demonstrates a reversible dihydrogen addition at ambient temperatures.[34] In the present work, we prepared several analogues of BorylCAT which contain various aryl substituents (phenyl, mesityl, 2-(isopropyl)phenyl) at the boryl site (Scheme 1). These di(aryl)boryl-substituted AABs, together with BorylCAT, constitute a series of isostructural compounds with varied electronic and, especially, steric properties of their Lewis acidic sites. We found that all these AABs add hydrogen with nearly neutral thermodynamics at close to ambient conditions. Moreover, we show that PHIP effects can be observed for these compounds under similar conditions. The influences of reaction kinetics, relaxation and scalar spin coupling parameters on the intensity of the PHIP signal is discussed in detail. Based on computational analysis of the BorylCAT–H_2 adduct, it is shown that the scalar spin coupling between the two protons originating from H_2 is the result of dihydrogen bonding and that borate (–BH_3) fragment rotation (libration) occurs.

2. Experimental

2.1 PHIP experiments

PHIP NMR experiments were performed on a Bruker AV 300 SB NMR spectrometer operating at 300 MHz ^1H resonance frequency and equipped with a broad-band 10 mm RF probe. The standard temperature control unit of the NMR spectrometer was used to maintain the desired temperature of the sample. The sample temperature was controlled by programmatically adjusted heating of a cold N_2 flow from a liquid nitrogen tank.

Commercially available high-purity H_2 gas was used for producing parahydrogen-enriched H_2, referred to below as "para-H_2". In this enrichment, H_2 from a gas cylinder was supplied through a spiral-shaped copper tube immersed in liquid N_2 at 77 K. The *ortho–para* conversion catalyst (FeO(OH)) was packed at the

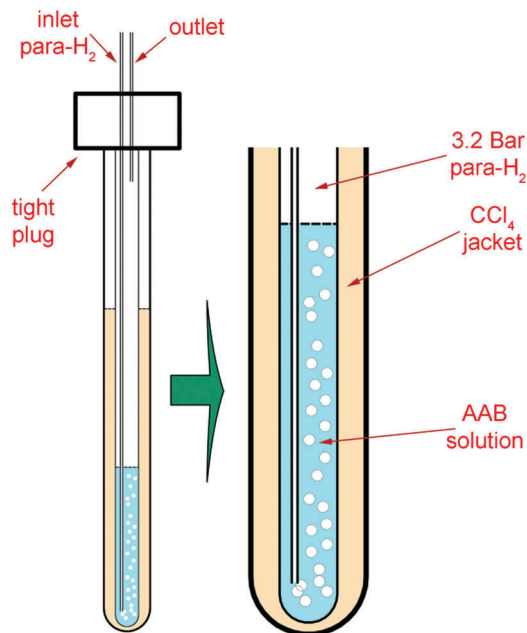This journal is © the Owner Societies 2016

Phys. Chem. Chem. Phys., 2016, **18**, 27784–27795 | 27785

Fig. 1 Experimental setup. A 5 mm NMR tube with AAB solution was fixed inside a heavy-wall 10 mm tube. A certain amount of CCl_4 was placed in the space between the walls of the tubes for better thermal stability. The bubbling of para-H_2 was performed using a thin PTFE capillary under a back pressure of 3.2 bar in order to obtain a higher para-H_2 concentration in the sample.

end of the spiral. As cooled H_2 flowed through the cold catalyst, parahydrogen-enriched H_2 with a 1:1 *ortho*:*para* ratio was produced for further use in the experiments.

In a typical workflow, a 5 mm sample tube (Wilmad) containing a ∼0.05 M solution of AAB in degassed dry methylene chloride-d_2 was placed inside the NMR magnet, and para-H_2, obtained as described above, was bubbled through the solution for 10 s. Then, the parahydrogen flow was abruptly terminated and the NMR experiment was started. ^{14}N decoupling (WALTZ16) was used for the acquisitions.

The 5 mm tube was fixed in a heavy-wall 10 mm tube including a CCl_4 jacket, stabilizing the temperature in the solution (Fig. 1). para-H_2 was supplied to the bottom of the sample tube through 1/32″ PTFE tubing under a pressure of 3.2 bar. The bubbling at elevated pressure resulted in a higher para-H_2 concentration (*ca.* 10^{-2} M) in the solution.

2.2 Measurements of kinetic and thermodynamic parameters

The measurements of kinetic constants were performed using the spin saturation transfer method[35–37] on a Bruker Avance III 600 MHz spectrometer. A heavy-wall 5 mm NMR tube equipped with a tight plug was used in the experiments. The samples were prepared by charging the tube with AAB solutions (∼0.05 M) and 5 bar of normal (thermal) H_2. ^{14}N decoupling (WALTZ16) was used for all acquisitions. The thermally polarized NH group proton signals were used to determine the rate constants for the dissociation of AAB–H_2 adducts into AAB and H_2 (k_{dis}, see eqn (1) in Section 4.2.1). The constants were calculated from the ratios of the signals in the normal spectra and in the spectra acquired

with presaturation of the ortho-H_2 resonance at *ca.* 4.6 ppm. In the latter case, the resonance of ortho-H_2 was irradiated (saturated) in a continuous wave mode for 30 s at the beginning of the pulse sequence. To determine k_{dis}, the following expression was used: $k_{dis} = (S_n/S_s - 1)/T_1^{NH}$, in which S_n is the signal intensity in the normal spectrum, S_s is the signal intensity in the spectrum with saturation, and T_1^{NH} is the relaxation time of the proton in the NH group. As the T_1 relaxation times of the NH and H_2 protons were significantly different, the standard inversion-recovery experiment was inappropriate for determining the correct value of T_1^{NH} because the chemical exchange couples the relaxation of the exchanging nuclei. To overcome this obstacle, the inversion-recovery experiment was replaced with the saturation-recovery protocol with irradiation of H_2 resonance during the recovery delays.

The AAB + H_2 equilibrium constants K_c (see eqn (4)) were determined from the ratios of the AAB, AAB–H_2 adduct and H_2 signals in the thermally polarized ^{1}H NMR spectra measured from the samples under 5 bar pressure of H_2. Concentration scaling was required for the conversion from signal amplitude units to concentrations; this was performed using the signal integrals and the known initial concentrations of the AABs. The association rate constant was derived as $k_{as} = K_c k_{dis}$.

Energetic parameters ($\Delta S^{\#}$ and $\Delta H^{\#}$) for the AAB–H_2 dissociation step were determined from the corresponding Eyring[38] plots using linear regression. The corresponding Eyring plots for the AAB compounds under study are shown in the ESI† (Fig. S5–S8).

2.3 Quantum chemical calculations

Density functional theory was applied to calculate the J_{HH} coupling constants between the NH and BH protons of BorylCAT–H_2 and ascertain the role of dihydrogen bonding. Coupling constants were calculated for several structures derived *via* the rotation of the BH_3 group in BorylCAT–H_2. Geometry optimizations and potential energy surface scan calculations were carried out at the ωB97X-D/6-311G** level of theory. ωB97X-D refers to the dispersion-corrected, range-separated hybrid exchange–correlation functional developed by Chai and Head-Gordon.[39–41] For numerical integrations, the ultra-fine integration grid was employed. The rotation of the BH_3 moiety was studied *via* potential energy surface scan calculations with respect to a dihedral angle involving the B–N bond; this was followed by transition state identification. J_{HH} coupling constants were computed for several conformers of BorylCAT–H_2 at the ωB97X-D/6-311G** level of theory using the Gauge-Independent Atomic Orbital (GIAO) method as implemented in Gaussian 09 software.[42]

To illustrate the presence of dihydrogen bonding, reduced density gradient (RDG) isosurface plots were generated using the NCIPLOT program for the optimized structure of BorylCAT–H_2 as well as for the rotational transition state.[43,44] The NCI (Non-Covalent Interactions) index enables real-space visualization of both attractive and repulsive interactions based on properties of the electron density.

27786 | *Phys. Chem. Chem. Phys.*, 2016, **18**, 27784–27795

This journal is © the Owner Societies 2016
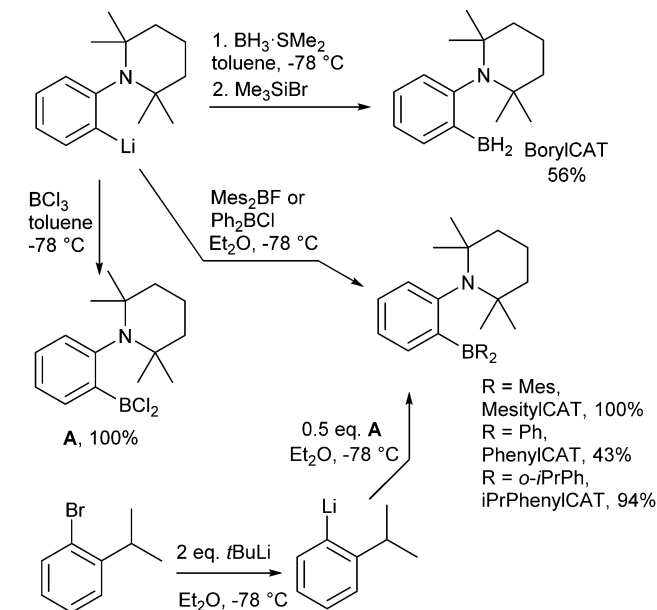
Scheme 2 Preparation of the AABs.

2.4 Synthesis of *ansa*-aminoboranes

BorylCAT was synthesized as described previously.[34] Diaryl-substituted *ansa*-aminoboranes were prepared as shown in Scheme 2. According to a modified procedure,[31] treatment of (2-(2,2,6,6-tetramethylpiperidin-1-yl)phenyl)lithium with dimesityl-fluoroborane or diphenylchloroborane in diethyl ether gave MesitylCAT and PhenylCAT in 100% and 43% yields, respectively. Addition of boron trichloride to the lithium compound afforded dichloroaminoborane A, which gave iPrPhenylCAT in 94% yield upon reacting with two equivalents of *ortho*-isopropyl-phenyllithium that were generated *in situ* by a Br–Li exchange of *ortho*-isopropylbromobenzene.

3. Results

Dihydrogen addition to AABs with different structures, which was investigated in this work using para-H$_2$, is represented by Scheme 3.

The scheme does not include nuclear spin dynamics and nuclear spin relaxation in AAB–H$_2$ because there is no obvious way to include these processes in chemical equations. Instead, they will be considered in subsequent discussions when it is required.
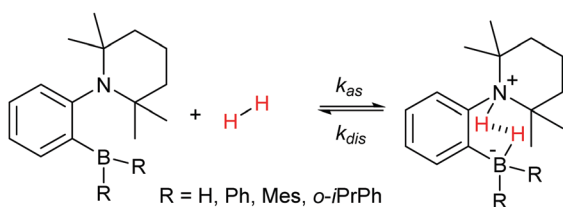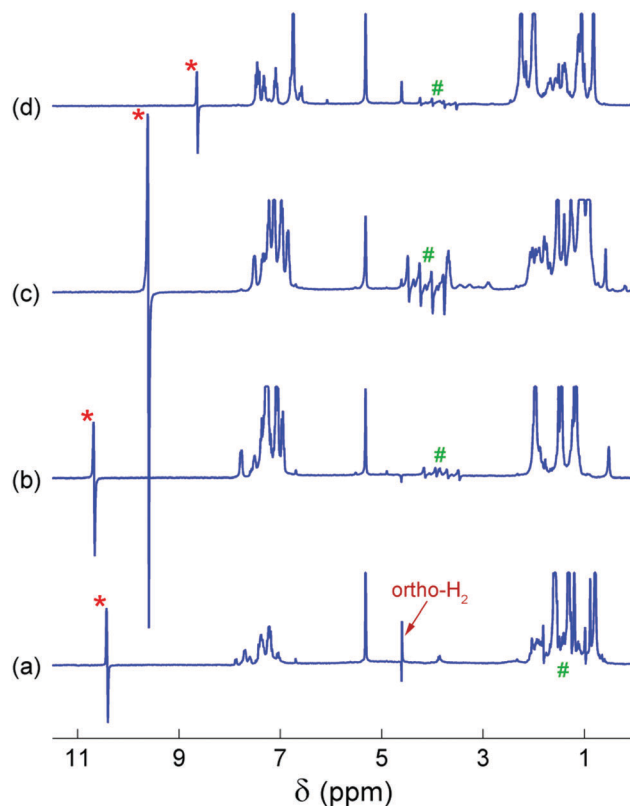

Scheme 3 Reversible activation of H$_2$ by the AAB compounds under study.

Fig. 2 ^{14}N-decoupled ^{1}H NMR spectra acquired at 20 °C in the experiments with BorylCAT (a), PhenylCAT (b), iPrPhenylCAT (c) and MesitylCAT (d). The antiphase PASADENA signals corresponding to the −NH and −BH groups are marked with "*" and "#", respectively.

The ^{14}N-decoupled ^{1}H NMR spectra acquired at 20 °C after bubbling para-H$_2$ through the AAB solutions are shown in Fig. 2. In all cases, characteristic antiphase (PASADENA-type) signals were observed for the NH and BH hydrogens in the NMR spectra (signal regions marked with "*" and "#", respectively). For an AX spin system of spin-1/2 nuclei, a single antiphase doublet would be expected in its spectrum. The shape of the NH signals is close to this conventional shape because the internal multiplet structure introduced by the spin-1 ^{14}N nucleus is collapsed due to the self-decoupling caused by a rapid spin relaxation of the ^{14}N nucleus. The amplitudes of the emissive (e) and absorptive (a) components of the antiphase doublet are not equal. This may be the result of the cross-relaxation occurring during the para-H$_2$ bubbling (for e > a)[28] or low hyperpolarization at low temperatures (for e < a); see Fig. S1–S4 (ESI†). In contrast, the polarized ^{1}H NMR signals of the BH group appear as a set of four antiphase doublets instead of a single doublet because of the splitting induced by the spin-3/2 ^{11}B nucleus.

In contrast to our previous study,[28] elevated temperature was not required here to observe polarization effects, meaning that PHIP can be produced at ambient temperatures with the AABs under study. Moreover, these effects were observed even at subzero temperatures (see below, and also Fig. S1–S4 in the ESI†). Comparison of the polarized signal intensities at room temperature reveals that the polarized signal intensity varied in

This journal is © the Owner Societies 2016

Phys. Chem. Chem. Phys., 2016, **18**, 27784–27795 | 27787

the following order: MesitylCAT < BorylCAT ≈ PhenylCAT < iPrPhenylCAT. Taking into account the steric hindrance introduced by the substituents at the boryl site, one could draw the conclusion that iPrPhenylCAT has optimal properties to produce polarization at room temperature, as the corresponding substituent is located between the highly hindered mesityl group and the moderately hindered phenyl group. However, due to the significant dependence of molecular processes on temperature, the H_2 addition process and, consequently, the polarization levels should exhibit a pronounced temperature dependence. To examine this, we performed experiments in which the temperature was varied in the range from −20 °C to 20 °C (see ESI,† Fig. S1 to S4). It was found that the intensity of the ^{1}H PHIP effect of the N–H···H–B hydrogen pair decreased gradually with decreasing temperature for BorylCAT, iPrPhenyl-CAT and MesitylCAT, whereas a clear maximum of PHIP was observed for PhenylCAT at *ca.* 0 °C (Fig. 3).

The existence of the maximum can be explained as the result of an interplay between the nuclear spin relaxation and reaction

Fig. 3 (a) ^{14}N-decoupled ^{1}H NMR spectra acquired after bubbling para-H_2 through a solution of PhenylCAT in methylene chloride-d_2 at different temperatures. NH and BH signal regions are displayed. (b) Bar chart of PHIP signal amplitudes for 0.05 M solutions of the given AABs at different temperatures. The bar stacks for different AABs are separated with dashed lines. The amplitudes were obtained from the NH proton signals. Additionally, the measured signal enhancements for these signals are shown with the numbers above each bar.

kinetics, as discussed in detail in Section 4.2.3. Briefly, for low H_2 addition rates (slow equilibrium establishment), nuclear polarization is destroyed by the relaxation, whereas at high addition rates, the relaxation is not significant, but the line broadening induced by the exchange diminishes the amplitude of the overlapping antiphase signals. Finally, at very high addition rates (very fast equilibrium establishment), nuclear spin correlation cannot efficiently evolve into observable polarization during the lifetime of the bound state of H_2. However, as discussed in Section 4.2.3, this simple explanation cannot exactly explain the position of the maximum if the experimentally measured relaxation times are taken into account.

The reaction kinetic parameters and the relaxation times were measured using the spin saturation transfer (SST)[35–37] method. The data are shown in Table 1. The details of the determination of the parameters are explained in Section 2.2.

4. Discussion

4.1 Dihydrogen-bond-mediated *J*-coupling in AABs as a prerequisite for PHIP

In this study, we used the so-called PASADENA experimental scheme,[25,45] *i.e.*, the reaction with para-H_2 was performed in a relatively high magnetic field (7 T). Under these conditions, the weak-coupling regime is fulfilled for all AAB–H_2 adducts of para-H_2, with the resonance frequency differences between the –NH and –BH protons (>1.2 kHz) in the adducts largely exceeding the *J*-coupling scalar constants (<6 Hz). The initial nuclear spin correlation of parahydrogen protons, also called the scalar spin order ($\sim I^{NH} \cdot I^{BH}$), transforms upon adduct formation into the longitudinal two-spin order ($\sim I_z^{NH} \cdot I_z^{BH}$)[45] because the transverse spin angular momentum components vanish due to decoherence induced by the resonance frequency differences. The $I_z^{NH} \cdot I_z^{BH}$ two-spin order can be transformed into the two-spin single quantum coherence orders ($I_z^{NH} \cdot I_x^{BH}$, $I_x^{NH} \cdot I_z^{BH}$, $I_z^{NH} \cdot I_y^{BH}$, $I_y^{NH} \cdot I_z^{BH}$) by a strong radio-frequency pulse of arbitrary phase, and a maximal amplitude is achieved if the pulse flip angle is equal to 45°. The latter orders cannot be observed in NMR directly, as NMR detection is only sensitive to single-quantum single-spin orders (I_x^{BH}, I_x^{NH}, I_y^{BH}, I_y^{NH}). Only these spin orders can contribute to the formation of transverse magnetization detected in practice. However, under the action of *J*-coupling interactions, the two-spin orders can evolve into observable magnetization.

It is clear from the above brief consideration that a nonzero spin–spin scalar constant between the –NH and –BH hydrogens is required to observe PHIP effects,[45] and the observation of these effects (Fig. 2) serves as evidence of a nonzero coupling constant.[28] However, the nature of this scalar coupling constant has been an open question. The *J*-coupling can be induced indirectly through the –N–C–C–B– molecular chain of the AABs. However, the typical values expected for a long-range [5]*J* constant are on the order of 1 Hz, which is much smaller than that observed experimentally (2.9 to 5.6 Hz, see Table 1). Previously,[28] we proposed that *J*-coupling in the H_2 adducts of
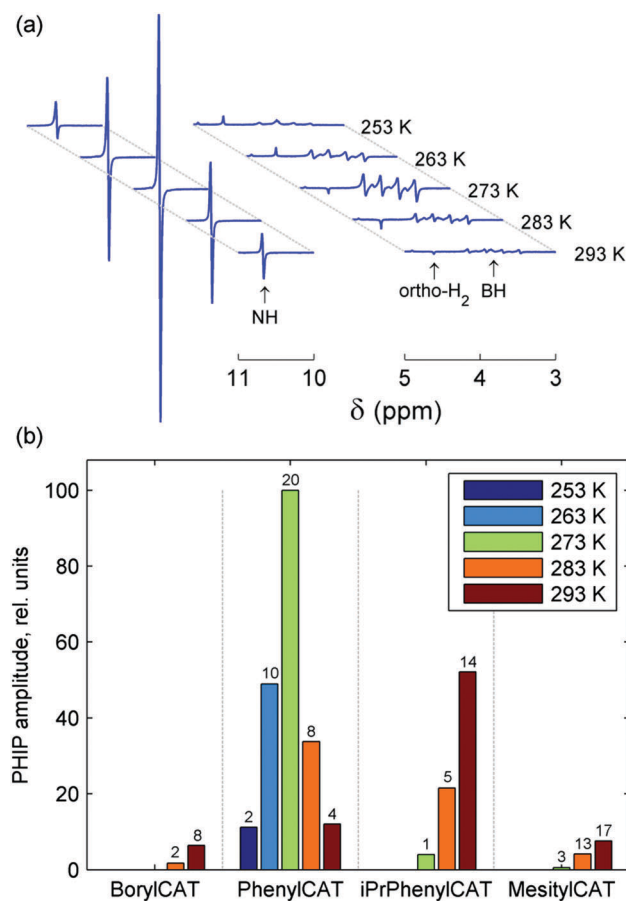
27788 | *Phys. Chem. Chem. Phys.*, 2016, **18**, 27784–27795

This journal is © the Owner Societies 2016

Table 1 Selected kinetic parameters, relaxation times and scalar coupling constants for BorylCAT, PhenylCAT, iPrPhenylCAT and MesitylCAT compounds as determined by NMR spectroscopy

AAB,[a] $\Delta H^{\#}$ (kcal mol^{-1}), $\Delta S^{\#}$ (cal mol^{-1})	T (K)	$k_{dis} \times 10^2$ (s^{-1})	$K_c \times 10^{-3}$ (M^{-1})	$^{NH}T_1$ (s)	$^{BH}T_1$ (s)	J_{HH} (Hz)	$\Delta \nu^e$ (Hz)
BorylCAT, 24.2 ± 2.9, 16.3 ± 9.1	273	0.1[b]	0.11[c]	0.73	—[d]	2.9	4.8
	283	0.4[b]	0.05[c]	0.88	—[d]	2.9	4.7
	293	1.1	0.03	1.07	—[d]	2.9	4.9
	303	7.6	0.01	1.21	—[d]	—	—
PhenylCAT, 21.3 ± 0.6, 15.0 ± 2.0	273	5.1	7.1	0.24	0.16	5.3	6.2
	283	38.2	2.1	0.28	0.2	5.3	5.9
	293	160.0	0.9	0.32	0.25	5.6	6.2
	303	540.2	0.3	0.38	0.29	—	—
iPrPhenylCAT, 22.9 ± 0.9, 13.4 ± 2.8	273	0.2[b]	3.2[c]	0.23	0.15	4.8	7.6
	283	1.0[b]	1.2[c]	0.30	0.16	4.8	6.5
	293	3.8	0.5	0.35	0.18	5.0	6.5
	303	17.9	0.2	0.42	0.23	—	—
MesitylCAT, 23.2 ± 7.7, 16.0 ± 25.7	273	0.5[b]	0.014[c]	0.34	0.16	4.3	6.2
	283	2.2[b]	0.005	0.38	0.17	4.2	4.9
	293	10.4	0.002	0.42	0.20	4.2	4.9
	303	32.2	0.001	0.49	—[d]	—	—

[a] $\Delta S^{\#}$ and $\Delta H^{\#}$ values corresponding to the dissociation rate constant k_{dis}. [b] The rate constant was predicted using the energetic parameters in the first column. [c] Equilibrium constants were calculated by extrapolating experimental data. [d] T_1 measurement was impossible to perform because the BH signal overlapped with other signals or it was very weak. [e] The full line width at half maximum determined for the NH proton signal.

AABs is likely direct in nature and may be induced by dihydrogen bonding between the –NH and –BH hydrogens.

DFT calculations carried out for the BorylCAT–H$_2$ adduct species provided further information on the origin of the J-coupling. The optimized structure of the BorylCAT–H$_2$ molecule features a short distance between the NH and BH hydrogens (1.44 Å), and the J_{HH} coupling constant is computed to be 6.2 Hz at this geometry.

Computations also reveal that the BH$_3$ group of the adduct can easily rotate (or undergo a librational motion) around the B–C bond, as the rotational barrier is predicted to be only 3.8 kcal mol^{-1} on the potential energy surface. We have therefore calculated the coupling constants along the rotational pathway, *i.e.* as a function of the C$_N$–C$_B$–B–H dihedral angle (see Fig. 4a). The results show a large variation of the J_{HH} values along the rotation. The coupling constant decreases rapidly as the H···H distance increases (it is 2.00 Å in the TS structure), suggesting that the J-coupling is induced by direct H···H interaction rather than *via* the covalent –N–C–C–B– linkage. The statistical averaging of the computed values gives 2.1 Hz for the coupling constant, which is in reasonable agreement with the experimentally observed value (2.9 Hz, see Table 1). Note that for other AABs, this rotation has much higher energy barriers and thus does not occur at ambient temperature.

To assess the nature of H···H interaction in the BorylCAT–H$_2$ adduct, we carried out NCI (non-covalent interactions) analysis by generating reduced electron density gradient isosurface plots for the ground state as well as for the rotational transition state (see Fig. 4b). In both structures, the blue regions between the NH and BH hydrogens reveal favorable (attractive) interactions, thus pointing to the presence of dihydrogen bonds. These results underline that dihydrogen bonding interactions play an important role in the observation of PHIP effects with AABs.

4.2 Reaction kinetics, nuclear spin relaxation and PHIP with AABs

In terms of the time scales involved, successful observation of PHIP effects (PASADENA in this work) requires a certain balance between reaction kinetics, nuclear spin relaxation and coherent spin dynamics to convert unobservable nuclear spin orders into observable ones. Any imbalance (*e.g.*, slow or very fast kinetics, slow spin dynamics or fast relaxation) will significantly decrease the observable polarization. The role of coherent spin dynamics requiring a nonzero J-coupling constant was discussed in Section 4.1. There is, however, another requirement: the value of the J-coupling constant must not be much smaller than the linewidth of the multiplet components, or the antiphase components will cancel each other out. The linewidth and the amplitude of the longitudinal two-spin order, in turn, are determined by the kinetic and relaxation parameters. To discuss this complex picture, it is convenient to consider the processes before and after the RF excitation pulse separately.

4.2.1 Evolution before RF pulse. Before the pulse, the experimental protocol included the bubbling of para-H$_2$ through AAB solutions. This process can be regarded as a stationary process that introduces a flux of para-H$_2$ nuclear scalar spin order (correlation) into the system. The correlation is transferred further to the AAB adduct with H$_2$ *via* intermolecular chemical exchange. A formal kinetic equation for the intermolecular exchange reads

$$\text{AAB} + \text{H}_2 \underset{k_{dis}}{\overset{k_{as}}{\rightleftharpoons}} \text{AAB} - \text{H}_2 \qquad (1)$$
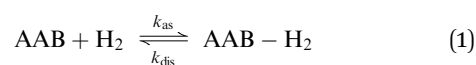
where k_{as} is the association rate constant and k_{dis} is the dissociation constant.

As was discussed in Section 4.1, the nuclear spin correlation originating from para-H$_2$ transforms into the two-spin order

(a)

(b)

BorylCAT-H₂   TS of BH₃ rotation
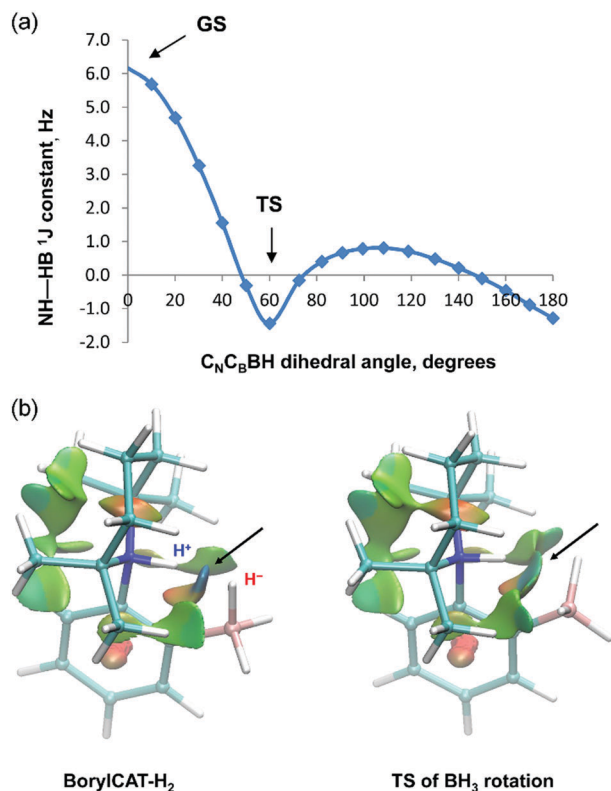
Fig. 4 (a) Theoretically predicted variation of the J_{HH} coupling constant in BorylCAT–H₂ as a function of the C_N–C_B–B–H dihedral angle (C_N and C_B denote the carbon atoms of the phenylene linker). The ground and the transition states (GS and TS) correspond to dihedral angles 0° and 60°. (b) Reduced electron density gradient (s) isosurface plots for BorylCAT–H₂ for the ground state and for the BH₃ rotation transition state (TS). Isosurfaces were generated for s = 0.3 a.u. and colored over the range $-0.07 < \rho < 0.07$ a.u. Blue color indicates attraction (dihydrogen bond, indicated by the arrows); the green and red regions correspond to very weak and repulsive interactions, respectively.

($I_z^{NH} \cdot I_z^{BH}$) in the adducts of AABs with para-H₂. It should be noted that in general, the efficiency of the transformation from the scalar spin order ($\mathbf{I}^{NH} \cdot \mathbf{I}^{BH}$) to only $I_z^{NH} \cdot I_z^{BH}$ depends on the difference between the resonance frequencies of the –NH and –BH protons, their mutual J-coupling constant, and the reaction rate constant (k_{dis} or k_{as}; they are interdependent under chemical equilibrium conditions). The frequency difference for all AABs in this study (>1.2 kHz) is much larger than the J-coupling constant and the rate constant, leading to the production of the $I_z^{NH} \cdot I_z^{BH}$ order with an efficiency close to 100% (see ESI†). Thus, continuous para-H₂ bubbling accompanied by intermolecular exchange leads to pumping of the $I_z^{NH} \cdot I_z^{BH}$ order with time, and the nuclear spin order amplitude reaches a stationary state at some point. In turn, the nuclear spin relaxation destroys the order. Therefore, the amplitude and the kinetics of the pumping process will depend on both the reaction rate constants and the nuclear spin relaxation parameters.

For simplicity, we assume that the para-H₂ flux into the solution is a fast process and that all free H₂ molecules in the solution are present in the form of para-H₂ under the stationary

conditions of para-H₂ bubbling. Moreover, we assume that the para-H₂/AAB/AAB–H₂ system is in chemical and magnetic equilibrium before the bubbling and that the Boltzmann polarization can be ignored due to its low amplitude. Then, if we mark the adduct molecules carrying non-equilibrium nuclear spin orders (e.g. $I_z^{NH} \cdot I_z^{BH}$) with "*", the kinetic equation determining the pumping process will be

$$\frac{d[AAB - H_2^*]}{dt} = k_{dis}\left([AAB - H_2]_0 - [AAB - H_2^*]\right) \\ - \left(\frac{1}{T_1^{BH}} + \frac{1}{T_1^{NH}}\right)[AAB - H_2^*] \quad (2)$$

Here, the first term on the right-hand side represents the $I_z^{NH} \cdot I_z^{BH}$ flux into AAB–H₂, the second term determines the destruction of the order by the nuclear relaxation, $[AAB-H_2]_0$ is the total concentration of the adduct, and $[AAB-H_2^*]$ is the instant concentration of the adduct molecules carrying the $I_z^{NH} \cdot I_z^{BH}$ nuclear spin order. Note that the relaxation process is assumed to be uncorrelated, meaning that the –NH and –BH protons relax independently. If, for simplicity, we group the relaxation constants into $1/T_1^* = 1/T_1^{BH} + 1/T_1^{NH}$, the solution of eqn (2) reads

$$[AAB - H_2^*](t) = [AAB - H_2^*]_0 \cdot \frac{1 - \exp\left(-\frac{1 + k_{dis} T_1^*}{T_1^*}t\right)}{1 + \frac{1}{k_{dis} T_1^*}} \quad (3)$$

One can see that the stationary state is approached with a function of the sum of the rates of chemical kinetics and nuclear spin relaxation, whereas the amplitude of the achievable $I_z^{NH} \cdot I_z^{BH}$ nuclear spin order is scaled by the factor determined by the parameter $k_{dis}T_1^*$. Note that $[AAB-H_2]_0$ and k_{dis} (and, much less sensitively, T_1^*) are temperature dependent. $[AAB-H_2]_0$ is essentially the equilibrium concentration of AAB–H₂ at a given temperature; thus, it can be expressed in terms of the reaction equilibrium constant (K_c) through the equation

$$K_c = \frac{[AAB - H_2]_0}{[AAB]_0[H_2]_0} \quad (4)$$

After solving $[AAB-H_2]_0$ from this equation and substituting it in eqn (3), the concentration of molecules carrying the $I_z^{NH} \cdot I_z^{BH}$ nuclear spin order over the bubbling time is determined by the following expression:

$$[AAB - H_2^*](t) = \frac{[AAB]_\Sigma}{1 + \frac{1}{K_c[H_2]_0}} \cdot \frac{1 - \exp\left(-\frac{1 + k_{dis} T_1^*}{T_1^*}t\right)}{1 + \frac{1}{k_{dis} T_1^*}}, \quad (5)$$

where $[AAB]_\Sigma$ is the total concentration of AAB in both forms (AAB and AAB–H₂). It can be seen that K_c and $[H_2]_0$ (which is essentially determined by the solubility of H₂ at a given temperature) influence the number of polarized molecules.

It should be noted that eqn (5) assumes that the para-H₂ singlet order is transformed to $I_z^{NH} \cdot I_z^{BH}$ with 100% efficiency in AAB–H₂ molecules; however, in general, this does not hold. Heuristically, eqn (5) can be equipped with the $I_z^{NH} \cdot I_z^{BH}$ amplitude

27790 | *Phys. Chem. Chem. Phys.*, 2016, **18**, 27784–27795

This journal is © the Owner Societies 2016

factor (f_{zz}) derived in the ESI† for chemically exchanging para-H_2 under stationary conditions for a two-spin system. Finally, the following formula for the maximum amplitude of $I_z^{NH} \cdot I_z^{BH}$ nuclear spin order acquired in the para-H_2 bubbling process is obtained:

$$[I_z^{NH} \cdot I_z^{BH}]_{max} = f_{zz} \cdot \frac{[AAB]_{\Sigma}}{1 + \dfrac{1}{K_c[H_2]_0}} \cdot \frac{1}{1 + \dfrac{1}{k_{dis}T_1^*}} \qquad (6)$$

The amplitude factor is

$$f_{zz} = \frac{\Delta\omega^2}{\Delta\omega^2 + J^2 + \left(\dfrac{k_{dis}}{2\pi}\right)^2} \qquad (7)$$

where $\Delta\omega$ is the resonance frequency difference between the –NH and –BH protons in Hz, whereas J is the scalar coupling constant between these protons in Hz. It should be noted that the derivation of eqn (7) assumed that k_{dis} is non-zero (see ESI†). The f_{zz} factor is very close to unity for all AAB adducts considered in this work and can be omitted in the following discussion. In general, however, we note that eqn (6) accounts for the spin dynamics (first term, f_{zz}), determining the efficiency of the singlet nuclear spin order transformation to $I_z^{NH} \cdot I_z^{BH}$; the chemical equilibrium (second term), determining the size of the AAB–H_2 pool; and, finally, the relaxation and the chemical exchange (third term), determining the overall amplitude. After the bubbling is stopped, the nuclear spin system will relax to magnetic equilibrium, reaching the Boltzmann polarization.

4.2.2 Evolution after the RF pulse. We assume that a $\pi/4$ RF pulse is applied just after the bubbling is stopped. As discussed in Section 4.1, this pulse will maximize the transverse magnetization signal derived from the pumped $I_z^{NH} \cdot I_z^{BH}$ nuclear spin order. In addition to the conventional transverse nuclear spin relaxation determined by T_2^*,[46] the chemical reaction (the H_2 exchange) will effectively contribute to the transverse relaxation, leading mainly to line broadening. Also, signal shape distortions may occur when the exchange rate is high.[47] Note that the exchange rates are not very high (Table 1), and extreme effects such as signal coalescence are not expected.

Let us first consider the line broadening, and assume for simplicity that we have an AX spin system. The evolution of the magnetization that resulted from the $I_z^{NH} \cdot I_z^{BH}$ nuclear spin order is detected as an antiphase Lorentzian doublet of the following shape:

$$\mathcal{L}_{anti}(\nu, \Delta\nu, J) \propto \frac{1}{4\pi} \cdot \frac{\Delta\nu}{(\nu - \nu_0 + J/2)^2 + \left(\dfrac{\Delta\nu}{2}\right)^2} - \frac{1}{4\pi}$$
$$\cdot \frac{\Delta\nu}{(\nu - \nu_0 - J/2)^2 + \left(\dfrac{\Delta\nu}{2}\right)^2} \qquad (8)$$

The integration of the absolute value of this shape gives the following integral intensity:

$$A_{anti} = \frac{2\tan^{-1}\left(\left|\dfrac{J}{\Delta\nu}\right|\right)}{\pi} \qquad (9)$$

where J is the scalar coupling constant and $\Delta\nu$ is the full line width at half maximum (FWHM) in Hz, determined as:

$$\Delta\nu \approx \frac{1}{\pi}\left(\frac{1}{T_2^*} + k_{dis}\right) \qquad (10)$$

Therefore, the reduction of the amplitude of the antiphase doublet may be dominated by either the transverse nuclear spin relaxation or the chemical kinetics. Note that $1/T_2^*$ has a weaker temperature dependence compared to k_{dis}. Thus, as the latter increases exponentially with increasing temperature, the PHIP signal decreases due to the reduction governed by the chemically induced line broadening. By combining eqn (9) and (10) with the maximum amplitude for $I_z^{NH} \cdot I_z^{BH}$ (eqn (6)), we obtain the following final expression for the amplitude of the antiphase signal after a $\pi/4$-pulse:

$$\text{Signal} \propto \frac{2\tan^{-1}\left(\left|\dfrac{\pi J}{1/T_2^* + k_{dis}}\right|\right)}{\pi} \cdot f_{zz} \cdot \frac{[AAB]_{\Sigma}}{1 + \dfrac{1}{K_c[H_2]_0}}$$
$$\cdot \frac{1}{1 + \dfrac{1}{k_{dis}T_1^*}} \qquad (11)$$

In addition to the line broadening effect, shape distortions such as accumulation of a complex phase may occur.[47,48] These effects, however, were not strong for the –NH and –BH signals. The exception was the signal of ortho-H_2, which had a dispersion component at certain temperatures in experiments with BorylCAT (see Fig. 2a and Fig. S1a, b in the ESI† and the discussion below).

4.2.3 Discussion of the experimental results. The experimental data can be analyzed in terms of eqn (11). As the f_{zz} factor is very close to unity (maximum) for any AAB studied in this work, it can be discarded from consideration. For the other three terms, we can identify the important dimensionless parameters determining the maximum observable antiphase PHIP signal as $\pi J/(1/T_2^* + k_{dis})$, $K_c[H_2]_0$ and $k_{dis}T_1^*$ for the first, third and fourth terms, respectively. These parameters were calculated and are given in Table 2 for selected temperatures. It should be noted that the total AAB concentration $[AAB]_{\Sigma}$ was the same in all cases and thus is not taken into consideration. However, it is obvious that increasing the AAB concentration will proportionally increase the antiphase PHIP signal. Numerical values of the PHIP signal attenuation factors corresponding to the given parameters are presented in Table S1 in the ESI.†

The first parameter, $\pi J/(1/T_2^* + k_{dis})$, determines the strength of the signal self-cancellation due to the line broadening of the overlapping antiphase components. Low values of J or a large sum of $1/T_2^* + k_{dis}$ will significantly diminish the observable antiphase PHIP signal. For the given AABs, the parameter did not exceed 0.9, meaning that at least 53% (see eqn (11) and Table S1 in the ESI†) of the polarized signal amplitude was lost due to the line broadening effect. The variation of this parameter from one AAB to another is not very significant, and we can conclude that the signal attenuation effect due to the line broadening was on the same order for all AABs. It should be noted that FWHM ($\Delta\nu$) values presented in Table 1 for the –NH

This journal is © the Owner Societies 2016

Phys. Chem. Chem. Phys., 2016, **18**, 27784–27795 | **27791**

Table 2 Characteristic parameters calculated for the AABs under study and the corresponding NMR signal enhancements observed in the PHIP experiments at selected temperatures

AAB	T (K)	$\pi J/(1/T_2^* + k_{dis})$	$K_c[H_2]_0$	$k_{dis}T_1^* \times 10^4$	Enh. factor[a]
BorylCAT	273	0.6	1.1	4.4	1
	283	0.6	0.5	18.5	2
	293	0.6	0.3	58.8	8.4
	303	—	0.1	459.8	—
PhenylCAT	273	0.8	71	49.0	20
	283	0.9	21	445.7	8
	293	0.9	9	2245.6	4
	303	—	3	8885.1	—
iPrPhenylCAT	273	0.6	32	2.0	1.2
	283	0.7	12	10.6	5
	293	0.8	5	45.2	14
	303	—	2	266.0	—
MesitylCAT	273	0.7	0.14	5.7	3
	283	0.9	0.05	26.1	13
	293	0.9	0.02	140.9	17
	303	—	0.01	457.3	—

[a] Experimentally measured enhancement factors, *i.e.*, ratios of hyperpolarized (after para-H$_2$ bubbling) and thermally polarized (after relaxation) signals.

proton resonances are on the order of 8 Hz, meaning that the sum of $1/T_2^* + k_{dis}$ is *ca.* 25 Hz (see eqn (10)). This relatively large number implies that the line broadening is primarily determined by T_2^* nuclear spin relaxation in the AAB molecules because k_{dis} does not exceed 1 Hz for the considered temperatures.

The second parameter, $(K_c[H_2]_0)$, determines the number of available AAB–H$_2$ molecules. This parameter controls the amplitude of the signal through the chemical equilibrium determined by thermodynamics. Larger K_c values or larger para-H$_2$ concentrations increase the overall signal. The former can be adjusted somewhat by varying the temperature, while the latter can be increased by performing experiments at high para-H$_2$ pressures to increase the concentration. Note that under the given experimental conditions, the parameter $K_c[H_2]_0$ varied in the following sequence: PhenylCAT > iPrPhenylCAT > BorylCAT > MesitylCAT (Table 2), meaning that thermodynamically, PhenylCAT is the best candidate for PHIP.

The third parameter $(k_{dis}T_1^*)$ is an intensive property which characterizes the strength of nuclear spin relaxation with respect to the rate of chemical exchange. A low value of this parameter indicates that either the nuclear spin relaxation is very fast or the reaction activity is weak, which leads to significant diminishing of the possible polarization levels. For every AAB in this study, this parameter was not high; however, it was more favorable in the case of PhenylCAT (Table 2).

The above discussion of the experimental data shows that the dimensionless parameters presented in Table 2 conveniently characterize the observed PHIP effects. They also can provide a good strategy basis for maximizing the polarization effects by using eqn (11) if the corresponding kinetic, thermodynamic and NMR parameters are known. Namely, the best results would be expected when $\pi J/(1/T_2^* + k_{dis}) > 4$, as the arctan function varies weakly once the argument value exceeds 4. Also, other

parameters should be $K_c[H_2]_0 \gg 1$ and $k_{dis}T_1^* \gg 1$ to minimize the respective denominators in eqn (11). These prerequisites, however, are not easy to fulfill in practice. The analysis has shown that the parameters for the considered AABs are far from optimal (see Table 2).

Moreover, the mechanistic features of H$_2$ activation may not be simple to describe. In particular, eqn (11) predicts that the maxima of antiphase PHIP signals should be observed at a certain temperature because $k_{dis}T_1^*$ decreases significantly at low temperatures, whereas $\pi J/(1/T_2^* + k_{dis})$ (and possibly $K_c[H_2]_0$) decrease significantly at high temperatures. This happens as a result of the exponential dependence of k_{dis} on temperature and qualitatively could explain the distinctive PHIP signal dependence obtained for PhenylCAT (Fig. 3). The position of the PHIP signal maximum, however, cannot be explained quantitatively using eqn (11). Fig. 5 compares the experimentally observed temperature of the PHIP signal amplitude maximum and the theoretically predicted temperature dependence of the PHIP signal amplitude for PhenylCAT. The fact that the positions of the two maxima do not match implies that some hidden dynamics occurs which displaces the experimental maximum to lower temperatures compared to the expected position. The nature of this effect is not clear; however, it may be related to the increase of thermodynamic variance at higher temperatures, defrosting a non-pairwise H$_2$ activation path. The latter process can occur in parallel to the pairwise path; however, in contrast, it does not lead to PHIP effects. Thus, the activation of a non-pairwise path could shift the temperature of the PHIP maximum toward lower temperatures. Another reason for the signal maximum shift may be the temperature sensitivity of the dihydrogen bond in AAB–H$_2$ molecules. The weakening of the dihydrogen bond at higher temperatures can cause the *J*-coupling between the NH and BH protons to vanish, leading to the disappearance of the PHIP
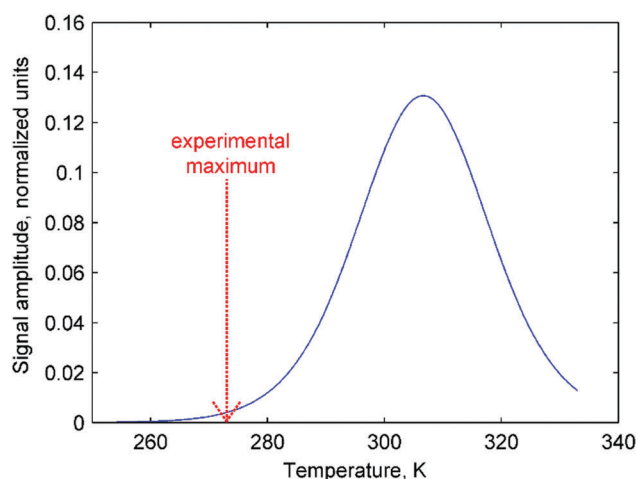
Fig. 5 Theoretically predicted antiphase PHIP signal amplitude as a function of temperature (eqn (11)) calculated using parameters for PhenylCAT from Table 2 (blue trace). [AAB]$_\Sigma$ parameter was set to unity in the calculation. Additionally, the position of the experimentally observed maximum of the PHIP signal amplitude is shown in the graph with a red dashed arrow.

27792 | *Phys. Chem. Chem. Phys.*, 2016, **18**, 27784–27795

This journal is © the Owner Societies 2016

effect (see Section 4.1). Additionally, in the derivation of eqn (11), we assumed that para-H_2 dissolution during the bubbling process is very fast, which may not be a good approximation and may cause some deviations.

Temperature dependence with a PHIP amplitude maximum was observed only for PhenylCAT; for the other AABs, the amplitude of the polarized signals gradually increased with increasing temperature (see Fig. 2 and Fig. S1–S4 in ESI†). This observation is in agreement with the theoretical expectations based on the parameters for BorylCAT, MesitylCAT and iPrPhenyl-CAT (Table 2). Higher temperatures are required to observe maxima for the latter compounds. BorylCAT, however, is somewhat different from the other AABs. In contrast to the others, at low temperatures, it demonstrated antiphase signals for two unknown polarized species in addition to those for BorylCAT–H_2 (see Fig. S1 in ESI†). The attempts to elucidate the structures of these species were not successful because of their very low concentrations. These species could be intermediates, side-products or impurities capable of activating H_2 in a pairwise manner, with N and B serving as active FLP centers.

Another peculiar finding for BorylCAT is the observation of a dispersive ortho-H_2 signal at elevated temperatures of 283 to 293 K (see Fig. 1a and Fig. S1a–c in the ESI†). This signal looks very similar to a signal with an antiphase shape; however, this shape is impossible for species where two protons have identical resonance frequencies, as in ortho-H_2.[27] Instead, the observed effect likely arises from a complex phase accumulation induced by a chemical exchange.[48] The exchange takes place between the protons captured in BorylCAT–H_2 and free H_2 molecules. After bubbling para-H_2 through BorylCAT solution followed by an RF pulse, free H_2 will still be present in the form of NMR-silent para-H_2, as it is insensitive to RF pulses. On the other hand, the proton pair in BorylCAT–H_2 will be polarized, and the polarization is transferred to free H_2 molecules after some time by the chemical exchange. The delayed appearance of ortho-H_2 molecules is equivalent to the accumulation of a complex phase for a particular NMR signal, which was observed experimentally in this study. This picture could explain our observations, but only qualitatively.

It was found using numerical spin dynamics simulations that the amplitude of the dispersive signal is very sensitive to the frequency differences between the H_2, –NH and –BH resonances (see Fig. S9 in the ESI†), and the large differences present for BorylCAT significantly decrease the amplitude of the dispersive ortho-H_2 signal. It is likely that a cross-correlated relaxation in BorylCAT–H_2 accompanied by chemical exchange may also have an influence on the dispersive ortho-H_2 signal by alternating the signal phase. This was indirectly confirmed by the observation of emissive ortho-H_2 signals (signals with negative amplitudes) at almost all temperatures in the experiments with BorylCAT; it can be explained in terms of the cross-correlated relaxation. Evidence that relaxation can convert an originally antiphase polarization to an in-phase (net) polarization is reported in the literature.[49,50] Moreover, similar emissive ortho-H_2 signals were observed in experiments with other AABs in this work (PhenylCAT), in our previous studies[28] on

metal-free H_2 activation, and also in experiments with diamagnetic Ru complexes.[50] As can be seen from the above discussion, a clear understanding of the peculiar subtle effects for ortho-H_2 signals requires separate exploration to be considered in full; this will be addressed in future works.

5. Conclusions

In conclusion, we have shown that all AABs studied in this work demonstrate the ability to provide PHIP. Moreover, the required reaction temperatures are close to ambient temperature; thus, the young field of FLP chemistry may bring the efficient production of nuclear spin polarization closer to realization. The experiments are not demanding, and, due to reversibility of H_2 addition to the AABs, the polarization can be observed after each cycle of parahydrogen bubbling. The experimentally measured kinetic, thermodynamic and NMR parameters allowed us to analyze the results with the aim of understanding current drawbacks. In particular, it was shown that nuclear spin relaxation accompanied by slow reaction kinetics significantly diminishes the nuclear spin polarization values. Moreover, the rapid nuclear spin relaxation increases the cancellation effect in the antiphase PHIP multiplets. One plausible solution for diminishing the influence of the nuclear spin relaxation would be the replacement of ^{14}N nuclei with ^{15}N. Eliminating the quadrupolar nucleus should increase T_1 as well as T_2 of the nuclear spins. The reaction kinetics issue can be improved by careful molecular design of the N–B FLP activation centers. The results obtained in this work clarify that variation of the substituents solely at the B-center significantly changes the reaction rates. However, as was found for Phenyl-CAT, increasing the reaction rates by increasing the temperature may not lead to the expected increase in signal enhancements because the activation of a non-pairwise reaction path or weakening of dihydrogen bonding may occur. Molecular "tuning" at the N-center would provide further flexibility in creating efficient AABs. Thermodynamically, PhenylCAT and iPrPhenylCAT have suitable characteristics, allowing close to quantitative conversion of the AAB molecules to the AAB–H_2 adducts, implying high concentrations of the hyperpolarized form of AAB–H_2. We believe that further rational investigation of the interactions between para-H_2 and AABs can lead to an efficient metal-free para-H_2 transfer to various substances and to high NMR signal enhancements. Meanwhile, the mechanistic information provided by PHIP shows that this class of molecules primarily activate H_2 molecules in a pairwise manner; demonstrations are already available for six different compounds, including the four studied in this work and two more in a study published earlier.[28] We are interested in both generating high levels of hyperpolarization and studying the AABs themselves, as they are unique. The observed hyperpolarization levels are not superior; however, we believe that the relevant improvements described above can provide efficient production of hyperpolarization with AABs. The theoretical analysis presented in the manuscript gives us and other researchers a direction and platform for

This journal is © the Owner Societies 2016

Phys. Chem. Chem. Phys., 2016, **18**, 27784–27795 | **27793**

further development. This analysis shows that for the systems studied here, the relevant kinetic and NMR parameters are suboptimal for observation of high hyperpolarization; however, this situation can be improved by further design of the AABs.

Acknowledgements

Notes and references

1 G. C. Welch, R. R. S. Juan, J. D. Masuda and D. W. Stephan, *Science*, 2006, **314**, 1124–1126.
2 G. C. Welch and D. W. Stephan, *J. Am. Chem. Soc.*, 2007, **129**, 1880–1881.
3 D. W. Stephan and G. Erker, *Angew. Chem., Int. Ed.*, 2015, **54**, 6400–6441.
4 D. W. Stephan, *J. Am. Chem. Soc.*, 2015, **137**, 10018–10032.
5 D. W. Stephan, *Acc. Chem. Res.*, 2015, **48**, 306–316.
6 D. W. Stephan, *Dalton Trans.*, 2009, 3129–3136, DOI: 10.1039/b819621d.
7 *Frustrated Lewis Pairs I: Uncovering and Understanding*, ed. G. Erker and D. W. Stephan, Springer Berlin Heidelberg, 2013.
8 *Frustrated Lewis Pairs II: Expanding the Scope*, ed. G. Erker and D. W. Stephan, Springer Berlin Heidelberg, 2013.
9 V. Sumerin, K. Chernichenko, M. Nieger, M. Leskelä, B. Rieger and T. Repo, *Adv. Synth. Catal.*, 2011, **353**, 2093–2110.
10 S. Grimme, H. Kruse, L. Goerigk and G. Erker, *Angew. Chem., Int. Ed.*, 2010, **49**, 1402–1405.
11 K. Chernichenko, Á. Madarász, I. Pápai, M. Nieger, M. Leskelä and T. Repo, *Nat. Chem.*, 2013, **5**, 718–723.
12 B. Waerder, M. Pieper, L. A. Körte, T. A. Kinder, A. Mix, B. Neumann, H.-G. Stammler and N. W. Mitzel, *Angew. Chem., Int. Ed.*, 2015, **54**, 13416–13419.
13 D. W. Stephan, S. Greenberg, T. W. Graham, P. Chase, J. J. Hastie, S. J. Geier, J. M. Farrell, C. C. Brown, Z. M. Heiden, G. C. Welch and M. Ullrich, *Inorg. Chem.*, 2011, **50**, 12338–12348.
14 D. W. Stephan, *Org. Biomol. Chem.*, 2012, **10**, 5740–5746.
15 J. Paradies, *Angew. Chem., Int. Ed.*, 2014, **53**, 3552–3557.
16 D. J. Scott, M. J. Fuchter and A. E. Ashley, *Angew. Chem., Int. Ed.*, 2014, **53**, 10218–10222.
17 S. Tussing, L. Greb, S. Tamke, B. Schirmer, C. Muhle-Goll, B. Luy and J. Paradies, *Chem. – Eur. J.*, 2015, **21**, 8056–8059.
18 M. Lindqvist, K. Borre, K. Axenov, B. Kótai, M. Nieger, M. Leskelä, I. Pápai and T. Repo, *J. Am. Chem. Soc.*, 2015, **137**, 4038–4041.
19 P. Eisenberger, B. P. Bestvater, E. C. Keske and C. M. Crudden, *Angew. Chem., Int. Ed.*, 2015, **54**, 2467–2471.

20 I. Chatterjee and M. Oestreich, *Angew. Chem., Int. Ed.*, 2015, **54**, 1965–1968.
21 Z. Zhang and H. Du, *Angew. Chem., Int. Ed.*, 2015, **54**, 623–626.
22 Á. Gyömöre, M. Bakos, T. Földes, I. Pápai, A. Domján and T. Soós, *ACS Catal.*, 2015, **5**, 5366–5372.
23 D. J. Scott, T. R. Simmons, E. J. Lawrence, G. G. Wildgoose, M. J. Fuchter and A. E. Ashley, *ACS Catal.*, 2015, **5**, 5540–5544.
24 Z. Zhang and H. Du, *Org. Lett.*, 2015, **17**, 6266–6269.
25 C. R. Bowers and D. P. Weitekamp, *J. Am. Chem. Soc.*, 1987, **109**, 5541–5542.
26 M. G. Pravica and D. P. Weitekamp, *Chem. Phys. Lett.*, 1988, **145**, 255–258.
27 J. Natterer and J. Bargon, *Prog. Nucl. Magn. Reson. Spectrosc.*, 1997, **31**, 293–315.
28 V. V. Zhivonitko, V.-V. Telkki, K. Chernichenko, T. Repo, M. Leskelä, V. Sumerin and I. V. Koptyug, *J. Am. Chem. Soc.*, 2014, **136**, 598–601.
29 L. E. Longobardi, C. A. Russell, M. Green, N. S. Townsend, K. Wang, A. J. Holmes, S. B. Duckett, J. E. McGrady and D. W. Stephan, *J. Am. Chem. Soc.*, 2014, **136**, 13453–13457.
30 F. Schulz, V. Sumerin, S. Heikkinen, B. Pedersen, C. Wang, M. Atsumi, M. Leskela, T. Repo, P. Pyykko, W. Petry and B. Rieger, *J. Am. Chem. Soc.*, 2011, **133**, 20245–20257.
31 K. Chernichenko, M. Nieger, M. Leskelä and T. Repo, *Dalton Trans.*, 2012, **41**, 9029–9032.
32 K. Chernichenko, M. Lindqvist, B. Kótai, M. Nieger, K. Sorochkina, I. Pápai and T. Repo, *J. Am. Chem. Soc.*, 2016, **138**, 4860–4868.
33 M.-A. Légaré, M.-A. Courtemanche, E. Rochette and F.-G. Fontaine, *Science*, 2015, **349**, 513–516.
34 K. Chernichenko, B. Kótai, I. Pápai, V. Zhivonitko, M. Nieger, M. Leskelä and T. Repo, *Angew. Chem., Int. Ed.*, 2015, **54**, 1749–1753.
35 R. L. Jarek, R. J. Flesher and S. K. Shin, *J. Chem. Educ.*, 1997, **74**, 978.
36 M. Montag, J. Zhang and D. Milstein, *J. Am. Chem. Soc.*, 2012, **134**, 10325–10328.
37 W. G. Wang, T. B. Rauchfuss, L. Y. Zhu and G. Zampella, *J. Am. Chem. Soc.*, 2014, **136**, 5773–5782.
38 P. W. Atkins and J. De Paula, *Physical chemistry*, W.H. Freeman, Oxford: Oxford University Press, New York, 9th edn, 2010.
39 J.-D. Chai and M. Head-Gordon, *Phys. Chem. Chem. Phys.*, 2008, **10**, 6615–6620.
40 J.-D. Chai and M. Head-Gordon, *J. Chem. Phys.*, 2008, **128**, 084106.
41 S. Grimme, *J. Comput. Chem.*, 2006, **27**, 1787–1799.
42 M. J. Frisch, G. W. Trucks, H. B. Schlegel, G. E. Scuseria, M. A. Robb, J. R. Cheeseman, G. Scalmani, V. Barone, B. Mennucci, G. A. Petersson, H. Nakatsuji, M. Caricato, X. Li, H. P. Hratchian, A. F. Izmaylov, J. Bloino, G. Zheng, J. L. Sonnenberg, M. Hada, M. Ehara, K. Toyota, R. Fukuda, J. Hasegawa, M. Ishida, T. Nakajima, Y. Honda, O. Kitao, H. Nakai, T. Vreven, J. A. Montgomery, J. E. Peralta, F. Ogliaro, M. Bearpark, J. J. Heyd, E. Brothers, K. N. Kudin, V. N. Staroverov, R. Kobayashi, J. Normand, K. Raghavachari,

27794 | *Phys. Chem. Chem. Phys.*, 2016, **18**, 27784–27795

This journal is © the Owner Societies 2016

A. Rendell, J. C. Burant, S. S. Iyengar, J. Tomasi, M. Cossi, N. Rega, J. M. Millam, M. Klene, J. E. Knox, J. B. Cross, V. Bakken, C. Adamo, J. Jaramillo, R. Gomperts, R. E. Stratmann, O. Yazyev, A. J. Austin, R. Cammi, C. Pomelli, J. W. Ochterski, R. L. Martin, K. Morokuma, V. G. Zakrzewski, G. A. Voth, P. Salvador, J. J. Dannenberg, S. Dapprich, A. D. Daniels, O. Farkas, J. B. Foresman, J. V. Ortiz, J. Cioslowski and D. J. Fox, *Gaussian 09, Revision A.02*, Gaussian, Inc., Wallingford CT.

43 E. R. Johnson, S. Keinan, P. Mori-Sánchez, J. Contreras-García, A. J. Cohen and W. Yang, *J. Am. Chem. Soc.*, 2010, **132**, 6498–6506.

44 J. Contreras-García, E. R. Johnson, S. Keinan, R. Chaudret, J.-P. Piquemal, D. N. Beratan and W. Yang, *J. Chem. Theory Comput.*, 2011, **7**, 625–632.

45 C. R. Bowers, in *Encyclopedia of Nuclear Magnetic Resonance*, ed. D. M. Grant and R. K. Harris, Wiley, Chichester, 2002, vol. 9, pp. 750–769.

46 M. H. Levitt, *Spin dynamics: basics of nuclear magnetic resonance*, John Wiley & Sons, Chichester, England, Hoboken, NJ, 2nd edn, 2008.

47 A. D. Bain, *Prog. Nucl. Magn. Reson. Spectrosc.*, 2003, **43**, 63–103.

48 R. O. Kühne, T. Schaffhauser, A. Wokaun and R. R. Ernst, *J. Magn. Reson.*, 1979, **35**, 39–67.

49 S. Aime, R. Gobetto and D. Canet, *J. Am. Chem. Soc.*, 1998, **120**, 6770–6773.

50 S. Aime, W. Dastru, R. Gobetto, A. Russo, A. Viale and D. Canet, *J. Phys. Chem. A*, 1999, **103**, 9702–9705.

This journal is © the Owner Societies 2016

Phys. Chem. Chem. Phys., 2016, **18**, 27784–27795 | 27795